Advanced Steel Construction – Vol. 19 No. 2 (2023) 166–176
DOI:10.18057/IJASC.2023.19.2.9

POST-FIRE BEHAVIOR OF CROSS-SHAPED STEEL REINFORCED CONCRETE COLUMNS: SIMULATION AND ANALYTICAL EXPRESSIONS

Tian-Gui Xu [1], Dun Liang [1], Sheng-Gang Fan [1, *] and Wei Li [2]

[1] *Key Laboratory of Concrete and Prestressed Concrete Structures of Ministry of Education, School of Civil Engineering, Southeast University, Jiulonghu Campus, Nanjing, China*
[2] *The IT Electronics Eleventh Design & Research Institute Scientific and Technological Engineering Corporation Limited, Shandong Branch, Jinan, China*
** (Corresponding Author: E-mail: 101010393@seu.edu.cn)*

ABSTRACT

In order to explore the behavior of cross-shaped steel reinforced concrete (SRC) columns after fire, the heat transfer analysis model and structural analysis model were established by ABAQUS software. The simulation results of the cross-shaped column were compared with the existing test results, in the aspect of the temperature distribution, time-temperature curve, failure mode, and load-displacement relationship after fire exposure. The results show that the simulation results agree well with the experimental results. The influence of critical parameters on residual bearing capacity coefficient k was discussed, which including constant heating duration, maximum heating temperature, concrete strength, yield strength of section steel, yield strength of rebars, limb thickness, effective column length, rebar diameter, and steel content. Finally, a simplified formula was proposed to calculate the residual bearing capacity of cross-shaped SRC columns after fire.

ARTICLE HISTORY

Received: 23 November 2022
Revised: 3 March 2023
Accepted: 9 March 2023

KEYWORDS

Steel reinforced concrete column;
Cross-shaped column;
After fire exposure;
Finite element analysis;
Residual bearing capacity calculation

1. Introduction

In recently, cross-shaped steel reinforced concrete (SRC) columns have been widely used in high-rise buildings. This structure possesses not only the characteristics of high bearing capacity, significant stiffness and flexible layout, but also more esthetical and higher space utilization than ordinary square column, as depicted in Fig.1. Unfortunately, high-rise building fires are not uncommon, posing a serious threat to people's safety. After exposed to fire, the strength and rigidity of the steel-concrete composite members are lost, so it is essential to re-evaluate the residual bearing capacity to take appropriate reinforcement measures to ensure that the structure can withstand the corresponding load [1-4] and continue to put into use. However, the core issue of repair assessment is how to determine the residual bearing capacity of the structure after fire, which has not been resolved yet.

Nowadays, the behavior of SRC columns at room temperature has been extensively investigated [5-8], leading to the development of various design codes, such as *Technical specification for steel reinforced concrete composite structures* (JGJ138-2001) [9] in 2001, *Technical specification of Steel-Reinforced Concrete Structures* (YB9082-2006) [10] in 2006 and *Code for design of composite structures* (JGJ138-2016) [11] in 2016 by China. At the same time, some scholars [12-13] have combined new materials with this structure, providing a new perspective for the application of SRC columns.

In general, SRC columns have a high proportion of steel components and thin layer of concrete cover, making them more vulnerable to damage than reinforced concrete columns when exposed to the same fire conditions. Some scholars have studied the fire-resistance of SRC columns at high temperature and made some achievements. Zheng and Han [14] carried out the fire resistance test of SRC columns and analyzed the effects of different parameters. It revealed that the fire resistance of SRC columns was significantly impacted by the section size and slenderness ratio. Han et al. [15-18] carried out the tests of square section SRC columns and beam-column joints at high temperature. The effect of stress distribution, explosion spalling of concrete, bonding between steel and concrete on its mechanical properties was analyzed. In these tests, SRC structure both show a good bearing capacity and ductility at high temperature. Young [19] investigated the behavior of axially restrained SRC columns at elevated temperatures. The fire resistance obtained from the finite element model was compared with the values in EC 4. The result showed that the EC4 was generally conservative for the axially restrained SRC columns. Ellobody [20] introduced the modeling process, and post-processing of circular section steel-concrete composite columns under fire, analyzed the influence of geometric defects, residual stress, material properties, and other parameters on the load-displacement relationship and fire resistance of composite columns to perfect the design criteria in the norm further.

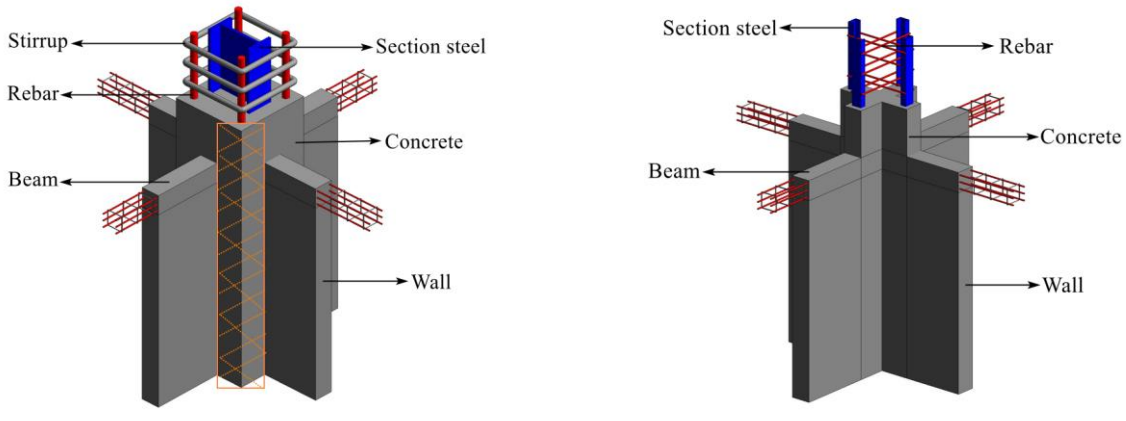

(a) (b)

Fig. 1 Steel Reinforced Concrete Columns: (a) Ordinary square column; (b) Cross-shaped column

Previous studies have shown that SRC columns have a good mechanical property at high temperatures, so this type of structure may still be put into use after exposure to fire. Therefore, the mechanical properties of SRC columns after exposure to high temperature have also attracted the attention of many experts and scholars. Zhang et al. [21], Meng et al. [22], Han et al. [23, 24], Chen et al. [25] and Liu et al. [26] investigated the behavior of square section steel-concrete composite columns after fire, revealed the relationship between temperature distribution and load-displacement. In addition, the effects of fire time, steel content, and other parameters that can influence the residual bearing capacity of columns were also considered. Yang et al. [27] carried out the compressive performance test of SRC short columns after exposure to high temper, and established the calculation formula of ultimate strength after fire. The proposed formula can better calculate the ultimate strength of short columns, but it has some limitations for the calculation of medium and long columns.

In summary, these research finds compensated for the deficiencies of existing studies, but the section type still was limited, mainly concentrate on square and circular, which cannot meet the needs of the research on special-shaped columns. There were few studies on the performance of SRC special-shaped columns after fire. The post-fire behavior of nine T-shaped SRC columns was studied by Wang et al. [28]. A formula for calculating the remain bearing capacity of T-shaped columns after high temperature was proposed. Liu et al. [29] completed the post-fire test of cross-shaped SRC columns. Due to the restriction of fire test cost and instrument, the parameter study of cross-shaped columns after exposure to high temperature was limited. However, in many aspects, such as maximum temperature, concrete strength, steel content, etc. will have unpredictable impact on the post-fire behavior of cross-shaped SRC columns. Accordingly, it is necessary to use the finite element method to analyze the performance of cross-shaped SRC columns after the fire.

In this paper, the ABAQUS [30] software was used to establish finite element models to analyze the fire effect of the cross-shaped SRC column. A series of systemic studies were carried out, including finite element simulation, parameter analysis and simplified design method, which can offer references for the repairing and strengthening of cross-shaped SRC columns after fire.

2. Test overview

2.1. Description of specimens

To further evaluate the post-fire behavior of cross-shaped SRC columns, the test data published by Liu et al. [29] was selected for comparison with the simulation results. Fig. 2 was the three-dimensional figure of the cross-shaped SRC columns with four 5 # section steel (50 mm × 37 mm × 4.5 mm × 7 mm, Cross-sectional area of section steel A_s= 692 mm^2). The rebar with a diameter of 8 mm was used as the web member to connect all the section steel. The high of column was 600 mm and limb thickness was 100 mm. In order to facilitate heating and loading, 200 mm high reinforced area were arranged at both ends of the column, as depicted in Fig. 3. The layout parameters details of cross-shaped columns are summarized in Table 1. Four temperature measuring points were arranged on the middle section of cross-shaped column, as illustrated in Fig. 4. These included measuring point 1 (the concave surface of the column), measuring point 2 (the center position), measuring point 3 (the inner margin of the steel web), and measuring point 4 (the convex surface), which were used to record the temperature-time history of the specimen. The specimen was heated at electric furnace, and kept different heating duration (60 min, 120 min and 180 min) at 600 ℃ as shown in Fig. 5.

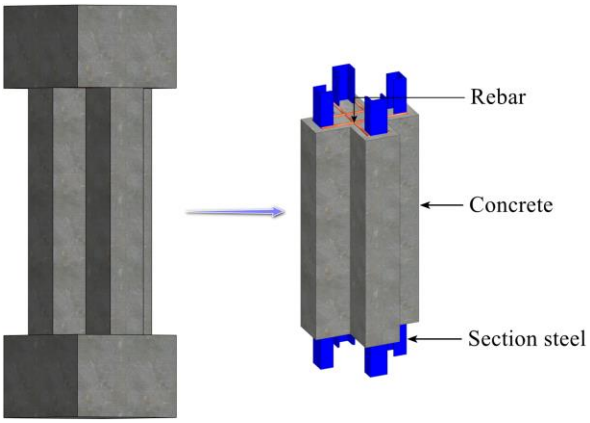

Fig. 2 Cross-shaped column three-dimensional figure

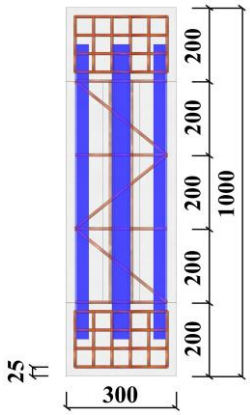

Fig. 3 Design drawing of steel skeleton

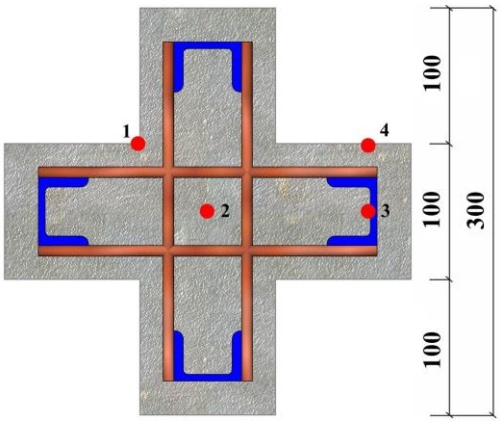

Fig. 4 Layout of measuring points

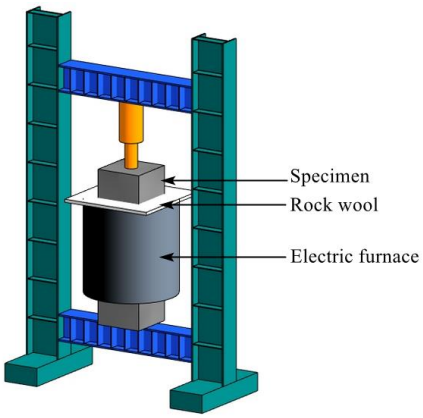

Fig. 5 Electric furnace for heating test

Table 1
Details of specimen parameters

Specimen	Constant heating duration (min)	Limb thickness (mm)	Effective length (mm)	Concrete strength (MPa)	Yield strength (Q235) (MPa)	Yield strength (HRB400) (MPa)
SRC-01	60	100	600	47.4	330	473
SRC-02	120	100	600	47.4	330	473
SRC-03	180	100	600	47.4	330	473

Table 2
The properties of concrete

Concrete coupon	Compressive strength (MPa)	Average compressive strength (MPa)	Young's modulus (GPa)	Average Young's modulus (GPa)
1	46.5		34.1	
2	48.5	47.4	34.7	34.4
3	47.2		34.6	

Table 3
The properties of steel

Steel type	Young's modulus (GPa)	Yielding strength (MPa)	Tensile strength (MPa)
5 # section steel	204	330	450
Rebar	205	473	615

2.2. Material properties

Liu et al. [29] conducted mechanical property tests on materials of concrete and steel. Table 2 summarizes the compressive strength and Young's modulus of concrete, while Table 3 provides the detailed test results of steel.

2.3. Test results

The experimental results carried out by Liu et al. [29] were summarized in this section. It was revealed that the temperature decreased with increasing depth of the measurement points and the thermal gradients reduced with increasing constant heating duration. The high temperature caused a reduction in the bond load between the concrete and section steel, leading to serious concrete falling off during the heating process, and all specimens exhibited shear failure mode under the load. Furthermore, the influence of heating duration on the bearing capacity of the specimen was studied. The results exhibited that both the cracking loads and ultimate loads decreased with increasing heating duration.

3. Finite element model

The thermal-mechanical coupling analysis of cross-shaped SRC columns under axial load after fire is complex. Two commonly used methods for this analysis are: the fully thermal-mechanical coupling method and the sequential thermal-mechanical coupling method. The former discussed the interplay between temperature development and stress, while the latter included the heat transfer stage and the structural analysis stage. Since the fully thermal-mechanical coupling method lacks computational efficiency and is difficult to converge when simulating complex structures, most scholars prefer the sequential thermal-mechanical coupling analysis method. The following four assumptions were set to simplify the simulation process: (1) the temperature distribution of steel is assumed to be uniform. (2) Ignore the thermal resistance among interfaces. (3) The deformation of steel and concrete is coordinated. (4) Ignore the concrete cover spalling.

3.1. Material constitutive

3.1.1. Thermal parameter

The thermal parameters of materials are the most basic data needed to simulate the temperature field, including density ρ, thermal conductivity λ_c, specific heat capacity C_c and Coefficient of thermal expansion α_c [31]. These thermal parameters will change with the increase in temperature. In recent years, scholars have proposed many methods to calculate the thermal performance of concrete and steel. The definitions of thermal parameters of steel and concrete were different in various countries fire resistance design codes. In the simulation test, the thermal parameters of steel and concrete were calculated by applying Eurocode 2 [32], Eurocode 3 [33] and Eurocode 4 [34].

3.1.2. Material properties of concrete

After fire, the various performance parameter of concrete is reduced greatly, and the stress-strain relationship also changes, as shown in Fig.6 (a). The influencing factors include not only the properties of aggregates and the strength of concrete, but also the external conditions such as heating rate, peak temperature, cooling method, etc. At present, many stress-strain relationship constitutive equations of concrete after exposure to fire have been derived by scholars. In this paper, the research results provided by Lu et al. [35] were adopted, and the constitutive equation was selected as follows.

$$y=\begin{cases}1-\varepsilon_{op}(T)\left(115(x-1)/(1+0.00504T)\right) & x\le 1\\ 2x-x^2 & x>1\end{cases} \tag{1}$$

where $x=\varepsilon_c/\varepsilon_{op}(T)$, $y=\sigma_c/\sigma_{op}(T)$ (2)

$$\sigma_{op}(T)=\sigma_o/\left(1+2.4(T-20)^6\times 10^{-17}\right) \tag{3}$$

$$\varepsilon_{op}(T)=\varepsilon_o\left(1+2.5\times 10^{-3}T\right) \tag{4}$$

where T is the highest temperature experienced; σ_c represents the stress of concrete and ε_c is the strain of concrete; σ_o and $\sigma_{op}(T)$ represent the peak stress of concrete at room temperature and after high-temperature, respectively; ε_o and $\varepsilon_{op}(T)$ represent the peak strain of concrete at room temperature and after high-temperature.

3.1.3. Material properties of steel

Compared with concrete, steel softens rapidly under fire. Steel strength declines significantly with the rise of temperature, while its lost strength will be substantially restored after cooling down. Fig.6 (b) indicates that the stress reduction of steel after the fire is minimal. Literature [36] pointed out that Poisson's ratio of steel is less affected by temperature. Therefore, this article assumes that the Poisson's ratio of steel remains unchanged after exposure to fire. The value of steel strength and elastic modulus in Eq. (5) adopts the suggestion of Wu [37], which are expressed as

$$\sigma_s=\begin{cases}E_{sr}(T)\varepsilon_s & \varepsilon_s\le\varepsilon_{yr}(T)\\ f_{yr}(T)+E_{sr}^{'}(T)\left(\varepsilon_s-\varepsilon_{yr}(T)\right) & \varepsilon_s>\varepsilon_{yr}(T)\end{cases} \tag{5}$$

$$f_{yr}(T)=\begin{cases}(100.19-0.01586T)\times 10^{-2}f_y & 20\ ℃<T<600\ ℃\\ (121.395-0.0512T)\times 10^{-2}f_y & 600\ ℃\le T<900\ ℃\end{cases} \tag{6}$$

$$E_{sr}(T)=(100.53-0.0265T)\times 10^{-2}E_s \qquad 20\ ℃<T\le 900\ ℃ \tag{7}$$

where σ_s and ε_s represent stress and strain of steel respectively; $\varepsilon_{yr}(T)$ represents the yield strain of steel after exposure to high-temperature; f_y and $f_y(T)$ are the yield strength of steel at ambient temperature and after high-temperature exposure, respectively; E_s and $E_{sr}(T)$ represent the elastic moduli of steel at ambient temperature and after high-temperature, respectively; $E_{sr}^{'}(T)$ represents the elastic modulus of the steel at the hardening stage after high-temperature, taking 1% of the elastic module of the specimen during the elastic phase.

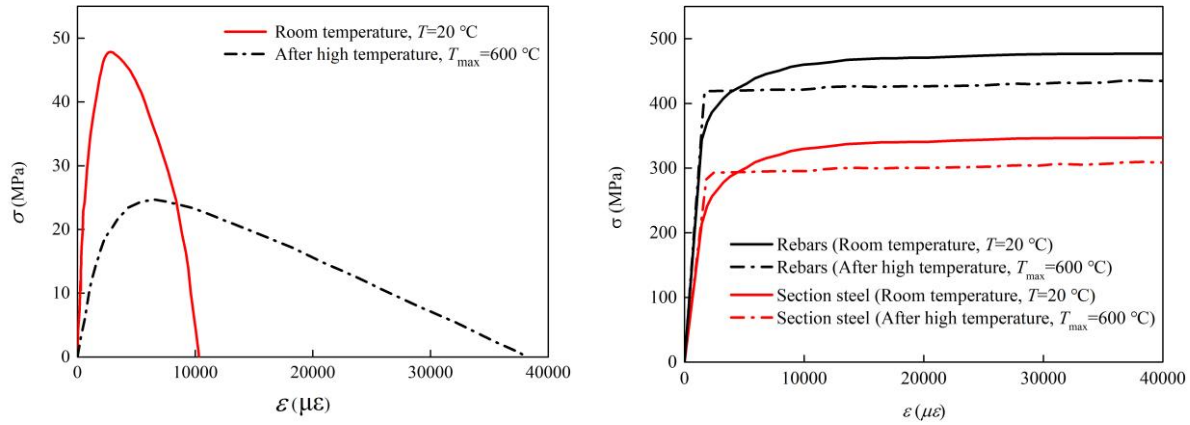

(a) (b)

Fig. 6 Stress-strain relationship of materials at different stages: (a) Concrete; (b) Steel

3.2. Heat transfer model

The temperature field modeling is a prerequisite for structural modeling. In the simulation test, the nonlinear heat transfer of cross-shaped columns was analyzed by using the finite element equation of energy conservation and the Fourier law of controlling heat conduction. Lie [38] revealed that the influence of rebars on heat transfer was small, so the role of rebars can be ignored in temperature field simulation. Note that the steels can be ignored in the temperature field analysis. When the temperature field was introduced into structural modeling, the steels can be added to the modeling and the temperature of the steels can be obtained by linear interpolation. Before the fire, the component was in the indoor environment, so the starting temperature of each point was 20 °C, the absolute zero was defined as -273 °C, and the Stefan-Boltzmann constant $\sigma = 5.67 \times 10^{-8}$ W / (m^2·K^4) was used.

The finite element mesh division needs to consider various conditions. As the element mesh is refined, the accuracy of the calculation results will be improved, but at the same time, the calculation efficiency will be reduced. Therefore, it is necessary to weigh various factors and conduct multiple tests to select the appropriate mesh division method. The maximum cell size of the grid density of the cross-shaped SRC columns was set as 20 mm in this test and the details of grid division as shown in Fig. 7.

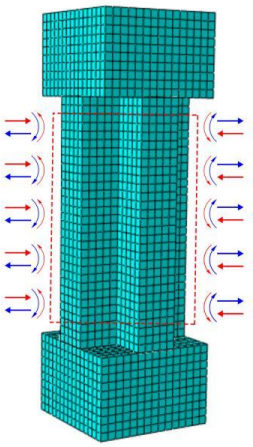

Fig. 7 Mesh model

The eight-node linear heat transfer hexahedral element DC3D8 was introduced to simulate concrete and section steel. The command "Tie" constraint was adopted between section steel and concrete, concrete and concrete without considering the influence of relative slip. The thermal convection and radiation boundary conditions were defined on the surface of the column according to Eurocode 4 [34]. The thermal radiation coefficient was defined as 0.7, and the convective heat transfer coefficient was defined as 25 W / (m^2·°C).

Fig. 8 shows the temperature distribution nephograms of cross-shaped columns at constant heating duration for 60 min, 120 min, and 180 min, respectively. It shows that the temperature of the column section decreases gradually from the outer surface to the center. The temperature near the section steel was basically similar. The temperature of the center of the column section was gradually increased with the rise of the constant heating duration.

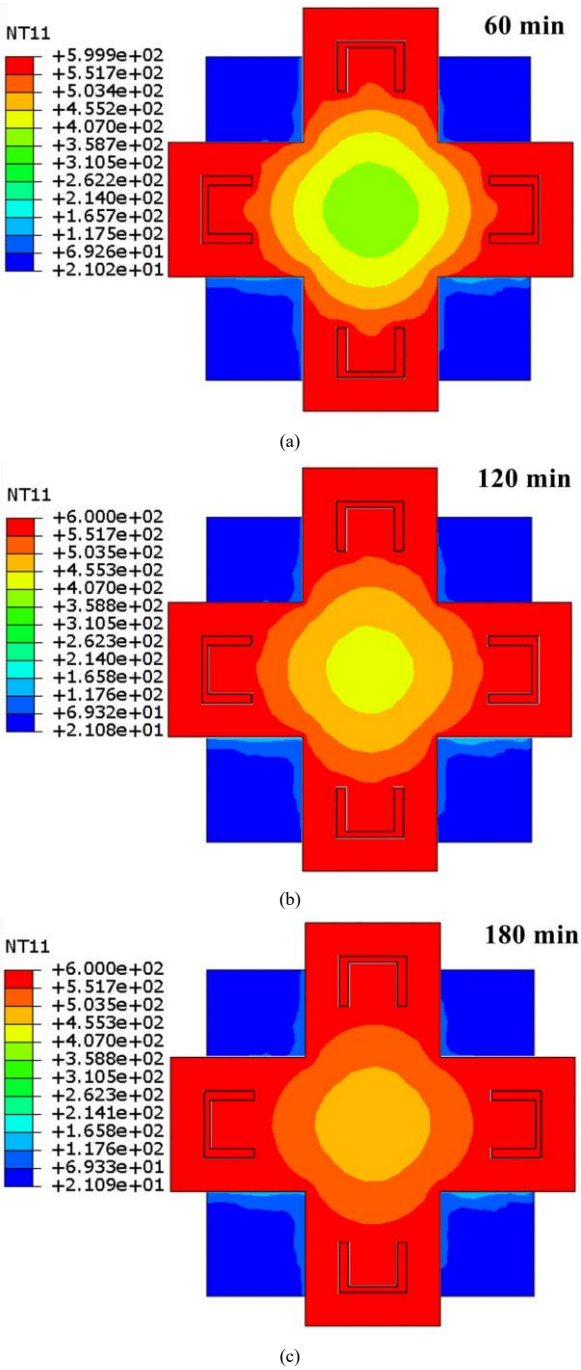

Fig. 8 The temperature field of different constant heating duration: (a) 60 min; (b) 120 min; (c) 180 min

3.3. Structural model

The thermal-mechanical coupling method was introduced to analyze the performance of cross-shaped SRC columns after fire. The secondary development of ABAQUS was carried out through Python, and the maximum temperature of each element node in the heat transfer process was extracted. Then the heat transfer analysis results were imported into the mechanical model to analyze the remain bearing capacity of the specimen after high temperature. It is necessary to keep the mesh division and node numbering consistent with the thermal field analysis model when establishing a mechanical finite element analysis model, so as to correctly read the temperature value of each node. Concrete and section steel were simulated by an eight-node three-dimensional solid linear shrinkage integral element (C3D8R), and rebars were affected by a three-dimensional truss linear element (T3D2).

The "Tie" constraint was assumed between section steel and concrete, and the "Embedded region" restriction was adopted between concrete and rebars. An external load was applied to the top connection point of the cross-shaped column by displacement. Since the initial geometric imperfection of cross-shaped columns was considered, the first elastic buckling mode of columns was multiplied by the amplification factor in the model, which is defined as L_s / 1000 [39], where L_s is effective column length.

The existing research [17] shows that the interface slip between concrete and section steel has a slight impact on the behavior of cross-shaped columns after fire, and thus was not taken into account in this paper.

4. Finite element verification

4.1. Temperature field analysis and verification

Fig. 9 shows the change of temperature-time histories of cross-shaped columns under different constant heating duration. The temperature rising trend of measuring point 2 was the slowest because of the longest conduction path of the cross-shaped column section. The rise in temperature of measuring point 4 was closest to the furnace temperature, which was caused by the direct exposure of the outer surface of the cross-shaped column to air. In the constant temperature stage, the difference in this temperature change trend was decreasing, because the concrete has a small heat transfer coefficient [29].

Fig. 9 demonstrates that the simulation can accurately predict the development of the time-temperature curve. At the start of heating process, the simulated temperature was similar to the result of the test. As temperature increased, the temperature rise trend of simulation and test was different. There are three main reasons: First, in the test process, when the concrete reaches about 100 °C, the water consumption energy will be evaporated, which retards the speed of the increase of temperature. Second, the contact between concrete and section steel is incomplete under fire, which produces certain thermal resistance in heat transfer [40], and the contact thermal resistance between concrete and section steel is ignored in heat transfer modeling. Third, concrete is essentially a discrete material, and concrete is usually regarded as a continuous medium in finite element simulation, resulting in the difference between the predicted temperatures and the measured results.

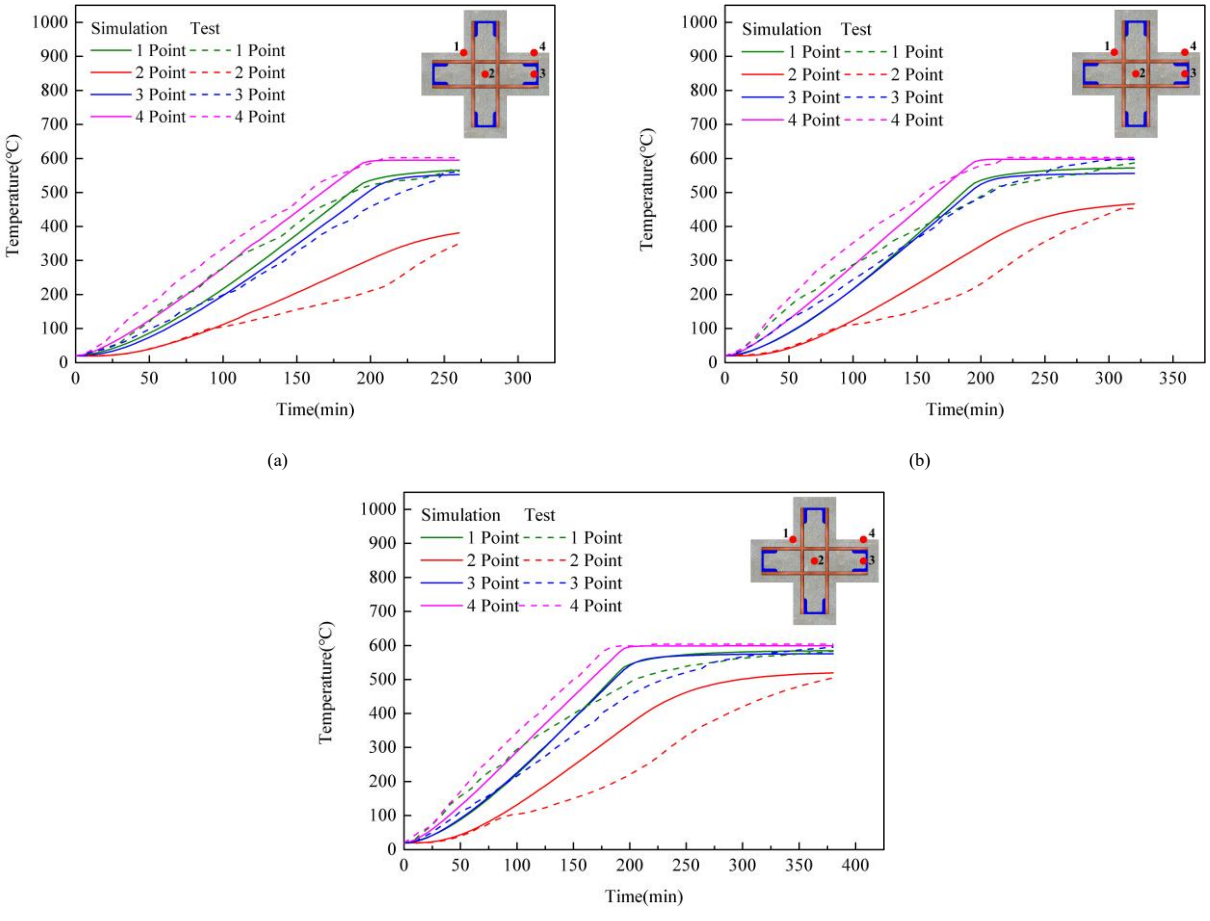

Fig. 9 Comparison of test and simulated temperature-time history: (a) Constant heating duration 60 min, (b) Constant heating duration 120 min, (c) Constant heating duration 180 min

4.2. Structural analysis and verification

Fig. 10 illustrates the failure modes between simulated and tested cross-shaped columns after fire. The simulated cloud picture shows the equivalent plastic strain of external concrete. The simulation results were found to be in agreement with the experimental results, and the simulation cloud picture of cross-shaped columns after fire shows a high lateral displacement in the middle. During the test, high-temperature heating caused the deterioration of concrete, resulting in the formation of vertical and oblique cracks under the load, mainly in the middle of the specimen. Therefore, the simulated strain distribution was basically consistent with the crack and shedding observed in the test.

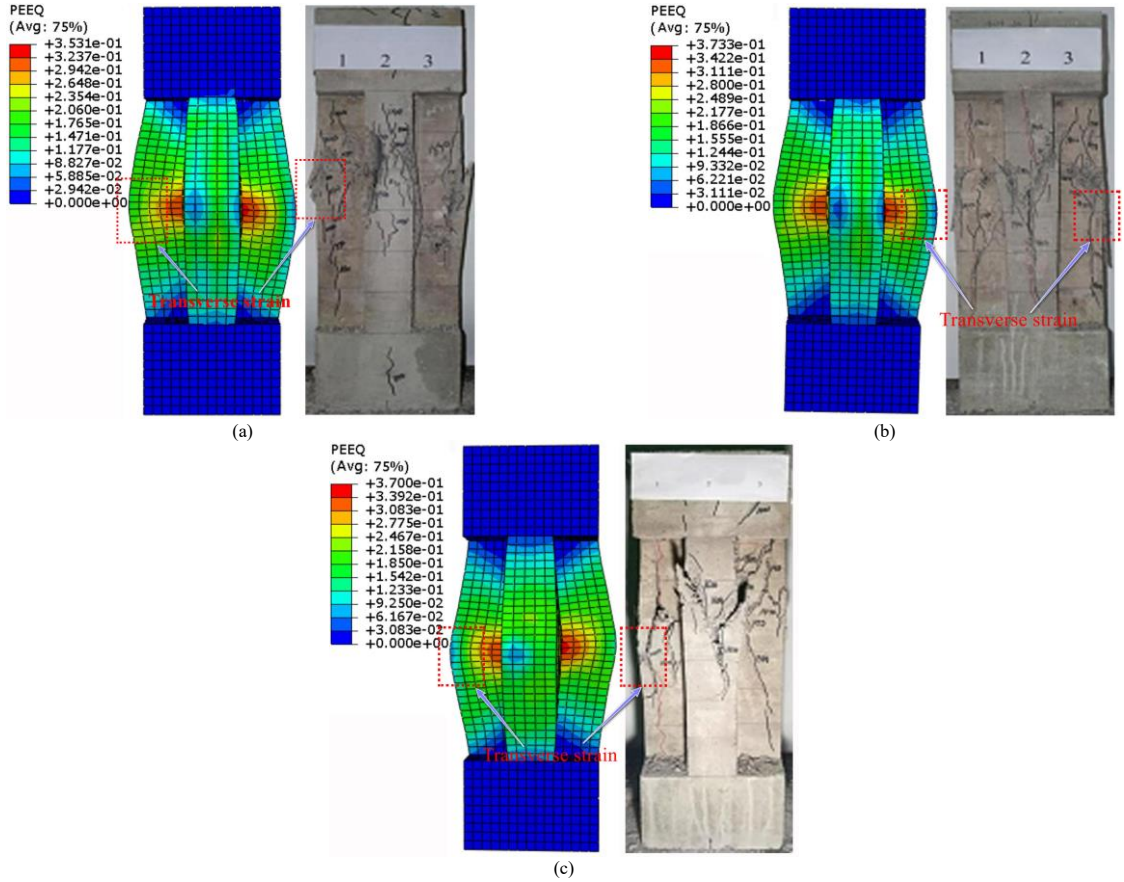

Fig. 10 Comparison of test results and simulated cloud picture: (a) SRC-01, (b) SRC-02, (c) SRC-03

The load-displacement curves of cross-shaped columns after fire is shown in Fig. 11. Under an axial load, the cross-shaped columns experienced the elastic stage, elastic-plastic stage, strengthening stage, descending stage, and residual stage. In the elastic stage, the deformation of concrete and section steel were coordinated, and no cracks appeared. In the elastic-plastic stage, concrete cracks appeared and expanded, section steel and rebars gradually yield. In the strengthening stage, the concrete was loose owing to the evaporation of free water in the internal pores of concrete after the fire. In the loading process, as the load increased, the loose concrete was gradually compacted, resulting in an increase in the stiffness of the column. In the descending stage, as the concrete protective layer continuously falls off, the bearing capacity of the column declines obviously. As displacement increases, the load drop tends to be gentle, and the residual bearing capacity was chiefly provided by concrete and section steel in the core zone in the residual stage. The load-displacement curves of the simulation and test of cross-shaped SRC columns is shown in Fig. 11. The finite element simulation of cross-shaped columns stiffness slightly overestimated the test value due to the lack of consideration of the influence of concrete spalling in the fire stage.

Table 4 compares the simulated and experimental results of the residual bearing capacity of cross-shaped SRC columns after fire. It shows that the average value and standard deviation of residual bearing capacity of cross-shaped columns were 1.016 and 0.007, respectively, indicating that the finite element model was effective.

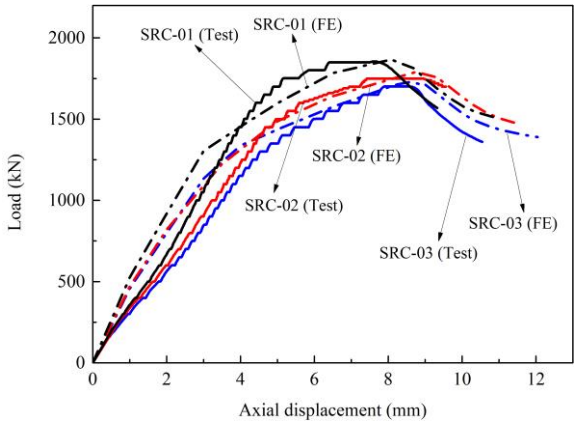

Fig. 11 Comparison between simulated and test values of load-displacement curves

Table 4
Comparison of residual bearing capacity between simulated and test values

Specimen	Constant heating duration (min)	Limb thickness (mm)	N_{FE} (kN)	N_{test} (kN)	N_{FE}/N_{test}
SRC-01	60	100	1863	1850	1.007
SRC-02	120	100	1790	1750	1.023
SRC-03	180	100	1732	1700	1.019
Mean value					1.016
Standard deviation					0.007

Note: N_{FE} represents the simulated value in kN, and N_{test} represents the test value in kN.

5. Effect of parameters on residual bearing capacity after fire

5.1. Parameter introduction

The critical parameters are set as shown in Table 5 for extended analysis, including constant temperature duration, maximum temperature, concrete strength, yield strength of section steel and rebars, limb thickness, effective column length, rebar diameter and steel content. Parameter values (Table 5) were selected according to Eurocode 4 [34] and practical engineering practices. These critical parameters were modeled using the same heating curve and boundary

conditions as the test.

Table 5
Parameters of the study

Parameter	Sign	Numerical value	Unit
Constant heating duration	t_c	60、120、180	min
Maximum temperature	T_m	600、700、800、900、1000	℃
Concrete strength	f_{cu}	20、30、40、50、60	MPa
Yield strength of section steel	f_y	215、235、345、390、420	Mpa
Yield strength of rebars	f_{yb}	335、400、500	Mpa
Limb thickness	L_e	100、150、200	mm
Effective column length	L_s	600、1000、1500、2000	mm
Rebar diameter	Φ	6、8、10	mm
Steel content	α	5.5、6.8、8.2	%

5.2. Definition of the residual bearing capacity coefficient

In order to estimate the residual bearing capacity of cross-shaped SRC columns after fire, the parameter k was introduced as the residual bearing capacity coefficient of cross-shaped SRC columns after fire, which is

$$N_u(t) = kN_u \tag{8}$$

where $N_u(t)$ represents the residual bearing capacity of cross-shaped SRC columns after fire; N_u represents the ultimate bearing capacity of cross-shaped SRC columns at ambient temperature.

5.3. Parametric analysis

The change of k value with the analysis parameters under different constant heating duration conditions is illustrated in Fig. 12. It shows that with the increase of constant heating duration, the residual bearing capacity of the cross-shaped SRC column decreases gradually, resulting in a significant decrease in the k value. Table 6 shows the range of k values corresponding to different analysis parameters under the conditions of constant heating duration of 60 min, 120 min, and 180 min (the difference between the maximum k value and the minimum k value). It can be seen from Table 6 that with the increase of constant heating duration, the range of k value was gradually reduced. In this paper, the average value of the range of k value was used as a reference, and divides the analysis parameters into two levels for description. Taking 15% of the range as the limit, greater than 15% was defined as the first-level parameter, and less than 15% was defined as the second-level parameter.

The first-level parameters include maximum temperature (T_m) and concrete strength (f_{cu}). Fig. 12 (a) displays that the k value declines with the rise of T_m, because the rise of T_m reduces the material behavior of the column. Besides, the downward trend of k value was also becoming more and more gentle, especially when the temperature rises from 900 °C to 1000 °C. This was because after T_m reaches 600 °C, the concrete protective layer has fallen off seriously. If the temperature continues to rise, the concrete will fall off less and less until it completely falls off.

Fig. 12 (b) shows that the value of k gets decreases as f_{cu} increases. The reason may be that the increase in concrete compressive strength leads to a decrease in internal porosity and a denser microstructure. Therefore, it becomes more difficult to release water vapor from the sample at high temperature, which leads to more serious degradation of material strength.

The second-level parameters include the yield strength of section steel (f_y) and rebar (f_{yb}), limb thickness (L_e), effective column length (L_s), rebar diameter (Φ), and steel content (α). From Fig. 12 (c) and Fig. 12 (d), it is evident that the value of k increases with the rise of steel yield strength. This is because the higher steel yield strength leads to an increase in the total plastic resistance of components. In addition, compared with the concrete strength (Fig.12 (b)), the increase of steel yield strength has slight influence on the k value, due to the steel strength has been dramatically restored during the cooling stage. The rise of f_{yb} has little impact on the value of k, and its range of less than 3% can be ignored.

Fig. 12 (e) shows that the k value increases with the increase of L_e. The reason was that the thermal inertia of concrete will increase with the rise of cross-section area, thereby reducing the temperature of the internal structure and improving the residual bearing capacity of columns.

Fig. 12 (f) displays that the k value declines with the rise of L_s, which was consistent with the research of buckling theory. In addition, the downward trend of the k value was more and more gentle, mainly because the increase of L may produce more residual deformation after exposure to fire, thereby increasing the second-order effect of load.

As can be seen in Fig. 12 (g) and 12 (h), the value of k increases with an increase in Φ or α. This was because higher Φ or α can improve the resistance to deformation of cross-shaped columns.

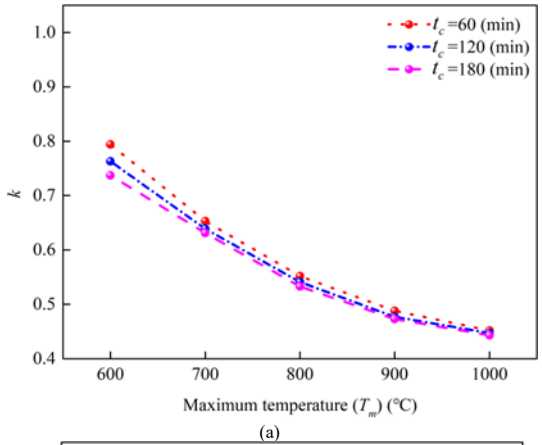

(a)

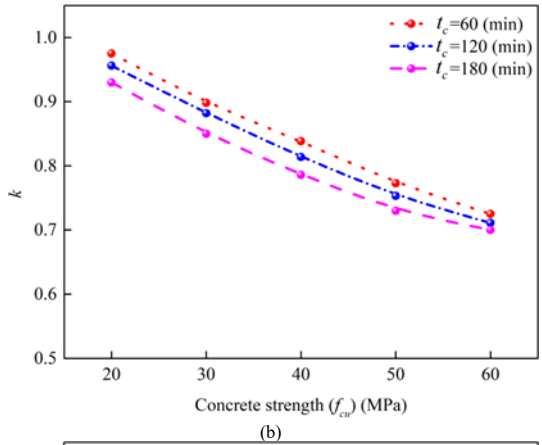

(b)

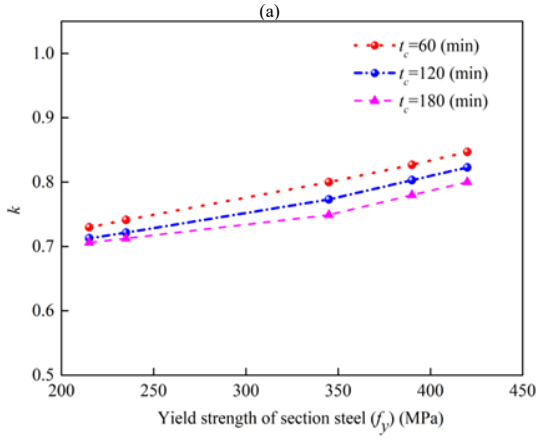

(c)

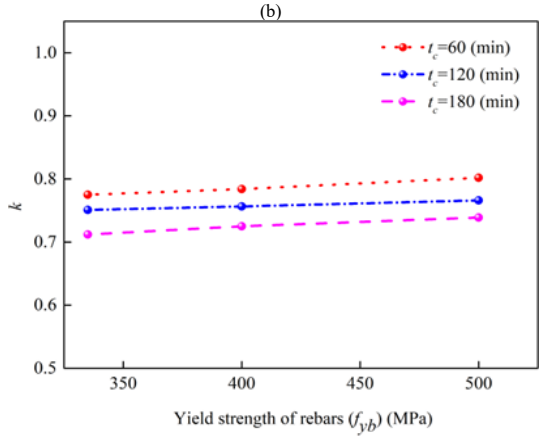

(d)

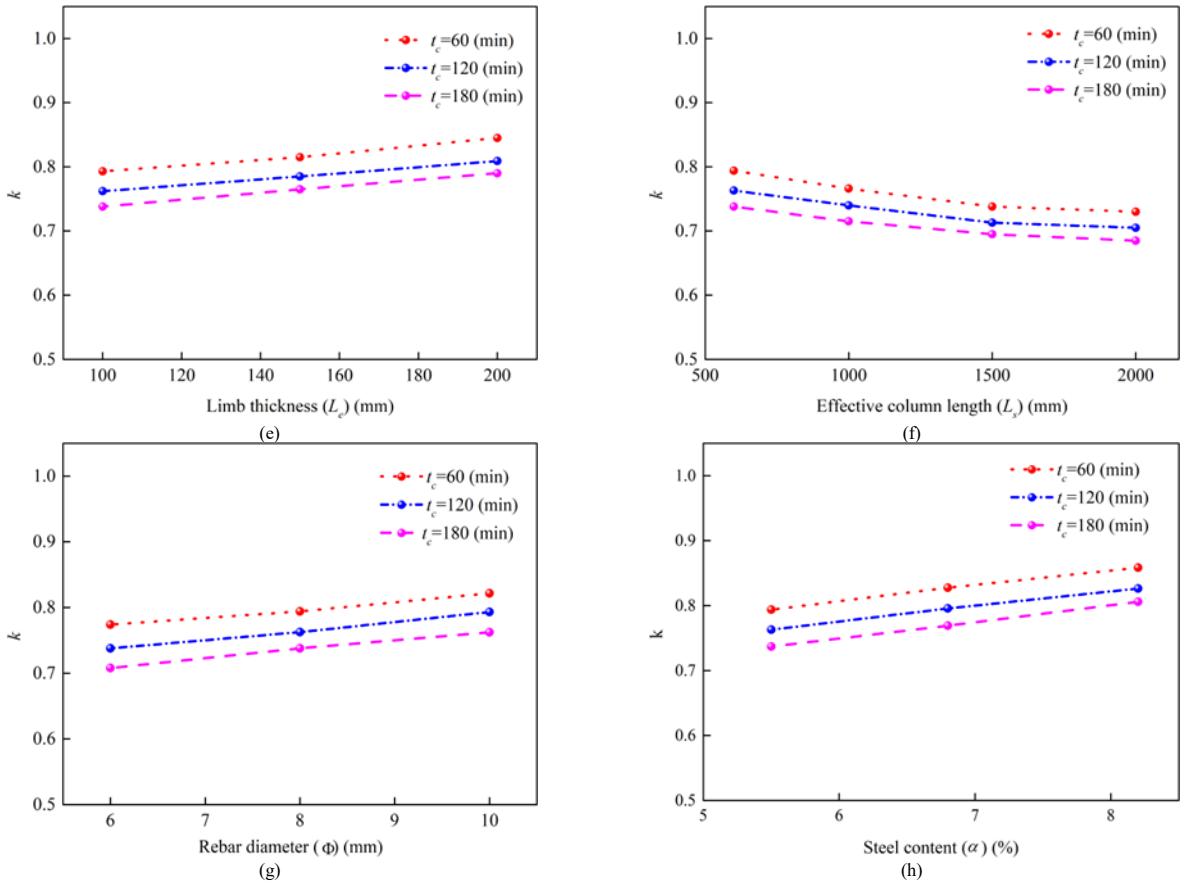

Fig. 12 Effect of parameters on the residual bearing capacity coefficient k: (a) Maximum temperature, (b) Concrete strength, (c) Yield strength of section steel, (d) Yield strength of rebars, (e) Limb thickness, (f) Effective column length, (g) Rebar diameter, (h) Steel content

Table 6
The variation of the range of k value with each analysis parameter under different constant heating durations

Parameter	Constant heating duration of 60 min	Constant heating duration of 120 min	Constant heating duration of 180 min	The mean value of the range of k
Maximum temperature	0.354	0.327	0.305	0.329
Concrete strength	0.250	0.245	0.233	0.243
Yield strength of section steel	0.117	0.110	0.074	0.100
Yield strength of rebars	0.027	0.015	0.027	0.023
Limb thickness	0.051	0.046	0.053	0.050
Effective column length	0.064	0.058	0.055	0.059
Rebar diameter	0.048	0.055	0.054	0.052
Steel content	0.064	0.063	0.069	0.065

6. Simplified design method

6.1. Temperature calculation formula

According to the simulation results, the temperature calculation formulas (20 ℃-1000 ℃) of each measuring point can be proposed respectively.

The temperature of measuring point 1 at the concave surface of cross-shaped columns can be calculated by the following formula:

$$T_{wc} = T_w + T_c \tag{9}$$

$$T_w = 1298.8 - 1470/\left(1+\exp\left((t_w - 211.7)/102.7\right)\right) \tag{10}$$

$$T_c = 40.3 - 16237.3/\left(1+\exp\left((t_c + 253)/41.8\right)\right) \tag{11}$$

$$T_m = 2131.1 - 37302/\left(1+\exp\left((T_w + 4461.2)/1577.8\right)\right) \tag{12}$$

where t_w and t_c is the heating time and constant heating duration, 20 min ≤ t_w ≤ 330 min, 10 min ≤ t_c ≤ 180 min. T_w and T_c are the temperatures of the heating section and constant temperature section, respectively, T_{wc} represents the measuring point temperature, T_m represents the ambient temperature around the column.

Measuring point 2 is situated in the middle of cross-shaped columns, and the temperature calculation formulas are as follows:

$$T_{wc} = T_w + T_c \tag{13}$$

$$T_w = 761.4 - 833.5/\left(1+\exp\left((t_w - 207.8)/86.8\right)\right) \tag{14}$$

$$T_c = 154.9 - 874.3/\left(1+\exp\left((t_c + 72)/47.3\right)\right) \tag{15}$$

$$T_m = 2211.3 - 19998.9/\left(1+\exp\left((T_w + 2158.1)/1017.9\right)\right) \tag{16}$$

Measuring point 3 is located in the inner edge of the steel web, which can be calculated by the following formula:

$$T_{wc} = T_w + T_c \tag{17}$$

$$T_w = 1386.7 - 1676 \Big/ \left(1 + \exp\left(\left(t_w - 208.65\right)/125.8\right)\right) \tag{18}$$

$$T_c = 45.15 - 29022.45 \Big/ \left(1 + \exp\left(\left(t_c + 127\right)/19.5\right)\right) \tag{19}$$

$$T_m = 3156 - 29141.5 \Big/ \left(1 + \exp\left(\left(T_w + 5150.3\right)/2418.6\right)\right) \tag{20}$$

The measuring point 4 is located on the convex surface of the cross column. The temperature of the concrete surface was nearly equal to the surrounding temperature during the heating stage, and remained relatively constant during the constant temperature stage. Therefore, the change of measuring point 4 temperature in the constant temperature stage can be ignored:

$$T_{wc} = T_w + T_c \tag{21}$$

$$T_w = 1542.6 - 2007.3 \Big/ \left(1 + \exp\left(\left(t_w - 186.5\right)/151.8\right)\right) \tag{22}$$

$$T_m = 7329.3 - 35192.5 \Big/ \left(1 + \exp\left(\left(T_w + 7647\right)/5703.6\right)\right) \tag{23}$$

6.2. Simplified calculation of ultimate bearing capacity at ambient temperature

In this paper, according to the method proposed by Eurocode 4 [34], and ignoring the constraint effect between section steel and concrete, the bearing capacity formula of cross-shaped SRC column at room temperature is derived as follows:

$$N_u = 0.9(\varphi_1 f_c A_c + 4\varphi_2 f_y A_s) \tag{24}$$

where φ_1 and φ_2 are the stability coefficients of cross-shaped columns, through the numerical fitting, φ_1 = 0.938, φ_2 = 0.931, f_c is the compressive strength of concrete at ambient temperature (f_c=0.79f_{cu}), f_y is the yield strength of steel at room temperature, A_c represents the cross-sectional area of the concrete cross-shaped column, and A_s is the cross-sectional area of single section steel.

6.3. Simplified calculation of the residual bearing capacity coefficient

The main parameters affecting the k value have been analyzed in the previous section. According to the numerical results in Fig. 12, the simplified formula of the k value is derived by the linear regression method:

$$k = \mu k_t k_{T_m} k_{f_{cu}} k_{f_y} k_{L_e} k_{L_s} k_\Phi k_\alpha \tag{25}$$

$$k_t = 0.8244\exp\left(-0.0006t\right) \qquad 30\ \text{min} \le t \le 180\ \text{min} \tag{26}$$

$$k_{T_m} = 1310.8T_m^{-1.16} \qquad 600\ ℃ \le T\ \le 1000\ ℃ \tag{27}$$

$$k_{f_{cu}} = 1.12\exp\left(-0.0072 f_{cu}\right) \qquad 20\ MPa \le f_{cu} \le 60\ MPa \tag{28}$$

$$k_{f_y} = 0.6261\exp\left(0.0007 f_y\right) \qquad 215\ MPa \le f_y \le 420\ MPa \tag{29}$$

$$k_{L_e} = 0.7448\exp\left(0.0006L_e\right) \qquad 100\ mm \le L_e \le 200\ mm \tag{30}$$

$$k_{L_s} = 1.2589L_s^{-0.072} \qquad 600\ mm \le L_s \le 2000\ mm \tag{31}$$

$$k_\Phi = 0.707\exp\left(0.0149\Phi\right) \qquad 6\ mm \le \Phi \le 10\ mm \tag{32}$$

$$k_\alpha = 1.4\alpha^{0.1957} \qquad 5.5\% \le \alpha \le 8.2\% \tag{33}$$

where k_t, k_{T_m}, $k_{f_{cu}}$, k_{f_y}, k_{L_e}, k_{L_s},k_Φ,k_α respectively represent the influence of constant temperature duration, maximum temperature, concrete strength, yield strength of section steel, cross-shaped columns section side length, effective column length, rebar diameter and steel content on the value of k. μ is stability factor, which takes 5.1.

6.4. Numerical comparison

Fig. 13 compares the time-temperature curve between the formula calculation results and the simulation results. It displays that those curves were very similar, which confirms the effectiveness of the temperature calculation method.

Fig. 14 displays the comparison between the k value calculated using the formula and the k value obtained from the simulation. The difference between the two values was within 10%, indicating that the formula-based method of calculating the k value was accurate within the given range.

Fig. 15 compares the calculated value of the formula in this paper with the calculated value of the formula proposed by Liu [29]. The calculation formula proposed in this paper can well envelope the test value of Liu. In addition, the calculation formula proposed in this paper is more applicable and has a wider parameter range than Liu's formula, as it does not require the temperature field distribution of the specimen to be determined before calculating the bearing capacity.

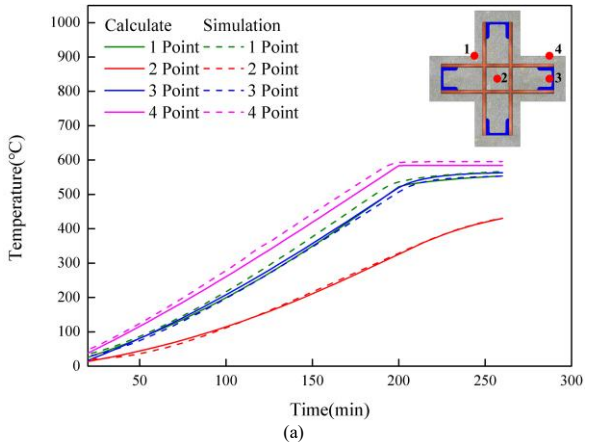

(a)

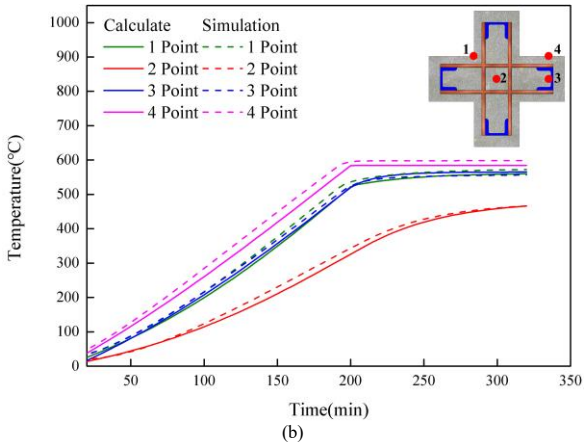

(b)

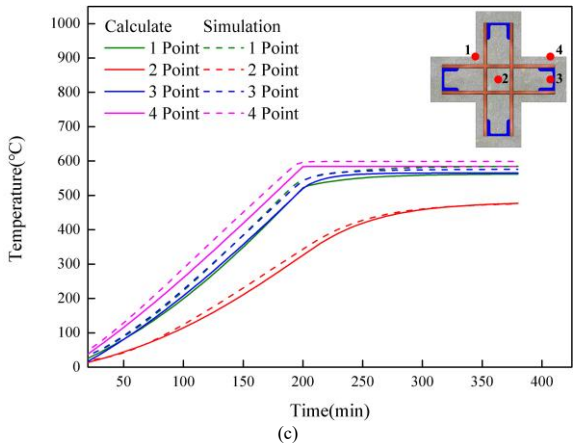

(c)

Fig. 13 Comparison of simulated and formula calculated temperature-time history: (a) Constant heating duration 60 min, (b) Constant heating duration 120 min, (c) Constant heating duration 180 min

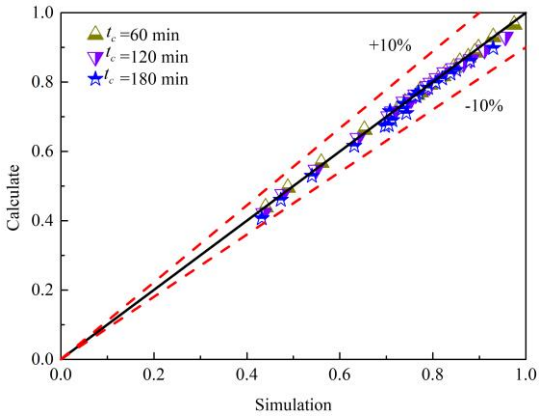

Fig. 14 Comparison of numerical analysis results and formula calculation results of *k* value

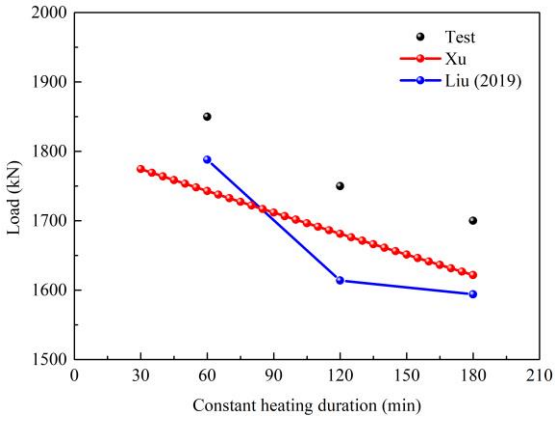

Fig. 15 Comparison of calculated load between different formulas

7. Conclusions

To further explore the post-fire behavior of cross-shaped SRC columns, a series of systemic studies were carried out in this paper, including test overview, finite element simulation, parameter analysis, and simplified design method. The following conclusions were obtained.

(1) The simulated equivalent plastic strain nephogram of the cross-shaped SRC column was compared with the actual failure diagram. The average value and standard deviation (1.016 and 0.007, respectively) of the residual bearing capacity of the cross-shaped SRC column after fire were calculated. It reveals that the finite element model is effective.

(2) The *k* value was gradually decreased with an increase in constant heating duration, maximum temperature, concrete strength, and effective column length. With the increase of yield strength of section steel, yield strength of rebar, limb thickness, rebar diameter, and steel content, the *k* value gradually increases.

(3) The concrete strength and the maximum temperature have the most significant influence on the *k* value. When the concrete strength is between 20 MPa and 60 MPa, the average value of the *k* value range is 24.3%. Similarly, when the maximum temperature is between 600 °C and 1000 °C, the average value of the *k* value range is 32.9%. The yield strength of reinforcement has the most negligible impact on the *k* value, where the range was less than 3%.

(4) The temperature calculation method of measuring points and the simplified calculation method of residual bearing capacity of the cross-shaped SRC column after fire were deduced. The calculation results were in good agreement with the finite element simulation results, which verifies the accuracy of the calculation method.

Declaration of competing interest

The authors state that they have no competing financial interests or personal relationships that could have influenced the work reported in this paper.

Acknowledgements

The authors are grateful for the financial support of The Open Fund of Shanghai Key Laboratory of Engineering Structure Safety (No. 2020-KF05) for sponsoring this research.

References

[1] Hou, L.F., Li, M., Liu, Y.C., “Numerical Simulation and Analysis of On-building High-rise Building Fires”, Procedia Engineering, 11, 127-134, 2011. DOI: 10.1016/j.proeng.2011.04.637

[2] Zhang, B.J., Wang, Y.Z., Li, G.Q., Qu, S., Fu, C.G., Xu, T.G., “Structural performance of steel reinforced concrete T-shaped columns exposure to high temperature”, Structures, 34, 716-728, 2021. DOI: 10.1016/j.istruc.2021.08.023

[3] Wang, Y.Z., Xu, T.G., Liu, Z.Q., Li, G.Q., Jiang, J., “Seismic behavior of steel reinforced concrete cross-shaped columns after exposure to high temperatures”. Engineering Structures, 230, 111723, 2021. DOI: 10.1016/j.engstruct.2020.111723

[4] Wang, Y.Z., Wang, X., Li, G.Q., Jiang, J., Xu, T.G., “Residual Strength of L-shaped Steel Reinforced Concrete Columns after Exposure to High Temperatures”, KSCE Journal of Civil Engineering, 25(4), 1369-1384, 2021. DOI: 10.1007/s12205-021-0658-9

[5] Cao X.L., Wu L.M., Li Z.M., “Behaviour of steel-reinforced concrete columns under combined torsion based on ABAQUS FEA”. Engineering Structures, 209, 109980, 2020. DOI: 10.1016/j.engstruct.2019.109980.

[6] Yang Y., Chen Y., Feng S.Q., “Study on behavior of partially prefabricated steel reinforced concrete stub T columns under axial compression”. Engineering Structures, 199, 109630, 2019. DOI: 10.1016/j.engstruct.2019.109630.

[7] Xiang S., Zeng L., Liu Y.H., Mo J.X., Ma L.L., Zhang J.C., Chen J., “Experimental study on the dynamic behavior of T-shaped steel reinforced concrete columns under impact loading”. Engineering Structures, 208, 110307, 2020. DOI: 10.1016/j. engstruct.2020.110307.

[8] Xue Y.C., Yang Y., Yu Y.L., “Shear strength model for steel reinforced concrete composite members: Short columns and deep beams”. Engineering Structures, 216, 110748, 2020. DOI: 10.1016/j.engstruct.2020.110748.

[9] JGJ138-2001. “Technical specification for steel reinforced concrete composite structures”, China Ministry of Construction, 2001. (in Chinese)

[10] YB9082-2006. “Technical specification of Steel-Reinforced Concrete Structures”, Nation Development and Reform Commission, 2006. (in Chinese)

[11] JGJ138-2016. “Code for design of composite structures”, China Ministry of Construction, 2016. (in Chinese)

[12] Dong H. Y., Zhu J., Cao W.L., Rao, Y.X., “Axial compressive behavior of mega steel-reinforced high-strength concrete columns with different steel sections”. Structures, 48, 1158-1174, 2023. DOI: 10.1016/j.istruc.2023.01.017.

[13] Lai B.L., Zhang. M.Y., Zheng X.F. Chen Z.P., Zheng, Y.Y., “Experimental Study on the Axial Compressive Behaviour of Steel Reinforced Concrete Composite Columns with Stay-in-Place ECC Jacket”. Journal of Building Engineering, 106174, 2023. DOI: 10.1016/j.jobe.2023.106174.

[14] Zheng, Y.Q., Han, L.H., “Calculations on the fire resistance of steel reinforced concrete (SRC)

columns", Fourth International Conference on Advances in Steel Structures, 2, 1017-1022, 2005. DOI: 10.1016/B978-008044637-0/50149-9
[15] Han, L.H., Tan, Q.H., Song, T.Y., "Fire Performance of Steel Reinforced Concrete (SRC) Structures", Procedia Engineering, 62, 46-55, 2013. DOI: 10.1016/j.proeng.2013.08.043
[16] Han, L.H., Tan, Q.H., Song, T.Y., "Fire Performance of Steel Reinforced Concrete Columns", Journal of structural Engineering, 141(4), 28-37, 2015. DOI: 10.1061/(ASCE)ST.1943-541X.0001081
[17] Han, L.H., Zheng, Y.Q., Tao, Z., "Fire performance of steel-reinforced concrete beam-column joints", Magazine of Concrete Research, 61(7), 499-518, 2009. DOI: 10.1680/macr.2008.61.7.499
[18] Song, T.Y., Han, L.H., Yu, H.X., "Temperature field analysis of SRC-column to SRC-beam joints subjected to simulated fire including cooling phase", Advances in Structural Engineering, 14(3), 353-366, 2013. DOI:10.1260/1369-4332.14.3.353
[19] Young, B., Ellobody, E., "Performance of axially restrained concrete encased steel composite columns at elevated temperatures", Engineering Structures, 33(1), 245-254, 2011. DOI: 10.1016/j.engstruct.2010.10.019
[20] Ellobody, E., "A consistent nonlinear approach for analyzing steel, cold-formed steel, stainless steel and composite columns at ambient and fire conditions", Thin-Walled Structures, 68,1-17, 2013. DOI: 10.1016/j.tws.2013.02.016
[21] Zhang, C., Wang, G.Y., Xue, S.D., Yu, H.X., "Experimental research on the behaviour of eccentrically loaded SRC columns subjected to the ISO-834 standard fire including a cooling phase", International Journal of Steel Structures, 16(2), 425-439, 2016. DOI: 10.1007/s13296-016-6014-0
[22] Meng, F.Q., Zhu, M.C., Mou, B., He, B.J., "Residual Strength of Steel-Reinforced Concrete-Filled Square Steel Tubular (SRCFST) Stub Columns After Exposure to ISO-834 Standard Fire", International Journal of Steel Structures, 19(3), 850-866, 2018. DOI:10.1007/s13296-018-0174-z
[23] Han, L.H., Zhou, K., Tan, Q.H., Song, T.Y., "Performance of steel reinforced concrete columns after exposure to fire: Numerical analysis and application", Engineering Structures, 211, 110421, 2020. DOI: 10.1016/j.engstruct.2020.110421
[24] Han, L.H., ASCE1, M., Zhou, K., Tan, Q.H., and Song, T.Y. "Performance of Steel-Reinforced Concrete Column after Exposure to Fire: FEA Model and Experiments", Journal of Structural Engineering, 142 (9), 55-67, 2016. DOI: 10.1061/(ASCE)ST.1943-541X.0001511
[25] Chen, Z.P., Liang, Y.H., Mo, L.L., and Ban, M.G., "Residual Properties and Axial Bearing Capacity of Steel Reinforced Recycled Aggregate Concrete Column Exposed to Elevated Temperatures", Frontiers in Materials, 7, 1-14, 2020. DOI: 10.3389/fmats.2020.00187
[26] Liu, F.Q., Yang, H., Yan, R., Wang, W., "Experimental and numerical study on behavior of square steel tube confined reinforced concrete stub columns after fire exposure", Thin-Walled Structures, 139, 105-125, 2019. DOI: 10.1016/j.tws.2019.02.037
[27] Yang, H., Yang, X., Mao, Z.H., "Compressive performance of steel-reinforced concrete columns after exposure to high temperature", Journal of Building Engineering, 59, 105120, 2022. DOI: 10.1016/j.jobe.2022.105120
[28] Wang, Y.Z., Gong J.L., Qu, S., Zhang B.J., Chen Y.T., "Mechanical properties of steel reinforced concrete T-shaped column after high temperature", Structures, 46, 852-867, 2022. DOI: 10.1016/j.istruc.2022.10.117
[29] Liu, Z.Q., Wang, Y.Z., Li, G.Q., Jiang, J., Fu, C.Q., "Mechanical behavior of cross-shaped steel reinforced concrete columns after exposure to high temperatures", Fire Safety Journal, 108, 102857, 2019. DOI: 10.1016/j.firesaf.2019.102857
[30] ABAQUS Standard Version 6.14 User's Manual, Volumes I-III Pawtucket, Dassault Systemes Simulia Corp, Rhode Island, USA, 2014.
[31] Hong, S.D., Varma, A.H., "Analytical modeling of the standard fire behavior of loaded CFT columns", Journal of Constructional Steel Research, 65(1), 54-69, 2009.
[32] EN l992-1-2, "Eurocode 2 Design of Concrete Structures", European Committee for Standardization, 2004.
[33] EN 1993-1-2, "Eurocode 3 Design of Steel Structures, Part 1.2: General Rules-Structural Fire Design", European Committee for Standardization, 2005.
[34] EN 1994-l-2, "Eurocode 4 Design of Composite Steel and Concrete Structures", European Committee for Standardization, 2005.
[35] Lu, Z.D., Zhu, B.L., Tan, W., "Study on reinforcement and repair of reinforced concrete beams after fire", Proceedings of the State Key Laboratory of Civil Engineering Disaster Prevention, 152-162, 1993. (in Chinese).
[36] Li, G.Q., Han, L.H., Lou, G.B., Jiang, S.C., "Fire design for steel and steel-concrete composite structures", Beijing: China Architecture and Building Press, 2006. (in Chinese).
[37] Wu, B., "Mechanical performance of reinforced concrete structures after exposure to fire", Beijing: Science Press, 2003. (in Chinese).
[38] Lie, T.T., "Fire resistance of circular steel columns filled with bar-reinforced concrete", Journal of Structural Engineering, 120(5), 1489-1509, 1994. DOI: 10.1061/(ASCE)0733-9445(1994)120:5(1489)
[39] Zhou, K., Han, L.H., "Modelling the behaviour of concrete-encased concrete-filled steel tube (CFST) columns subjected to full-range fire", Engineering Structures, 183, 265-280, 2019. DOI: 10.1016/j.engstruct.2018.12.100
[40] Ghojel, J., "Experimental and analytical technique for estimating interface thermal conductance in composite structural elements under simulated fire conditions", Experimental Thermal and Fluid Science, 28(4), 347-354, 2004. DOI: 10.1016/S0894-1777(03)00113-4